Multimodality bronchoscopic imaging of tracheopathica osteochondroplastica

Henri Colt
Septimiu D. Murgu
University of California School of Medicine
Pulmonary and Critical Care Medicine
Department of Medicine
101 the City Drive South
Building 53, Room 119
Route 81 Orange, California 92868
E-mail: hcolt@uci.edu

Yeh-Chan Ahn
Matt Brenner
University of California, Irvine
Beckman Laser Institute
1002 Health Sciences Road
Irvine, California 92612

Abstract. Results of a commercial optical coherence tomography system used as part of a multimodality diagnostic bronchoscopy platform are presented for a 61-year-old patient with central airway obstruction from tracheopathica osteochondroplastica. Comparison to results of white-light bronchoscopy, histology, and endobronchial ultrasound examination are accompanied by a discussion of resolution, penetration depth, contrast, and field of view of these imaging modalities. White-light bronchoscopy revealed irregularly shaped, firm submucosal nodules along cartilaginous structures of the anterior and lateral walls of the trachea, sparing the muscular posterior membrane. Endobronchial ultrasound showed a hyperechoic density of 0.4 cm thickness. optical coherence tomography (OCT) was performed using a commercially available, compact time-domain OCT system (Niris System, Imalux Corp., Cleveland, Ohio) with a magnetically actuating probe (two-dimensional, front imaging, and inside actuation). Images showed epithelium, upper submucosa, and osseous submucosal nodule layers corresponding with histopathology. To our knowledge, this is the first time these commercially available systems are used as part of a multimodality bronchoscopy platform to study diagnostic imaging of a benign disease causing central airway obstruction. Further studies are needed to optimize these systems for pulmonary applications and to determine how new-generation imaging modalities will be integrated into a multimodality bronchoscopy platform. © 2009 Society of Photo-Optical Instrumentation Engineers. [DOI: 10.1117/1.3155524]

Keywords: multimodality optical imaging; bronchoscopy; optical coherence tomography; endobronchial ultrasound; tracheopathica osteochondoplastica.

1 Introduction

The purpose of this report is to describe the appearance of excessive bronchial cartilaginous growth, as seen in a patient with tracheopathica osteochondoplastica (TPO), using a multimodality platform that includes white-light bronchoscopy, endobronchial ultrasound, and optical coherence tomography. In addition to reviewing the clinical and pathophysiologic features of this disease, the advantages and disadvantages of a multimodality bronchoscopic imaging system are presented, and potential future roles for these techniques are discussed.

2 Case Presentation and Methods

A 61-year-old nonsmoking Korean woman presented with a four-month history of dry cough. The patient denied dyspnea, hemoptysis, fever, chills, weight loss, or other symptoms. Past medical history was unremarkable, and she had no occupational or environmental exposures. Her physical examination, chest radiograph, and pulmonary function tests were normal.

Tuberculin skin testing was positive at 10 mm, but induced sputum stains were negative for acid fast bacilli. A computed tomography scan showed partial airway obstruction from extensive nodularity and thickening of the anterior and lateral tracheal walls in the setting of normal lung parenchyma and mediastinum [Fig. 1(a)]. White-light flexible bronchoscopy performed through a rigid 12-mm EFER-Dumon bronchoscope (Bryan Corps, Woburn, Massachusetts) revealed white, irregular, and firm nodules overlying the cartilaginous rings within the subglottis and along the anterior and lateral tracheal walls [Fig. 1(b)].

Airway wall extension was then studied using real-time endobronchial ultrasound (BF-UC260F; Olympus Optical Co. Ltd., Tokyo, Japan) with a 7.5-MHz radial probe [Fig. 1(c)]. In order to further characterize airway wall architecture at higher resolution, optical coherence tomography was performed using a compact, commercially available optical coherence tomography (OCT) system (Niris® Imaging System, Imalux® Corp., Cleveland, Ohio) with a two-dimensional, forward-imaging, flexible probe. The Niris System attributes include: Z-axis (depth resolution) of $10-20~\mu$m (in air), lat-

Address all correspondence to: Henri Colt, MD, UCI Medical Center, 101 the City Drive South, Bldg 53, Rm 119, Rt 81, Orange, CA 92868. Tel: 714-456-5150; Fax: 714-456-8349; E-mail: hcolt@uci.edu
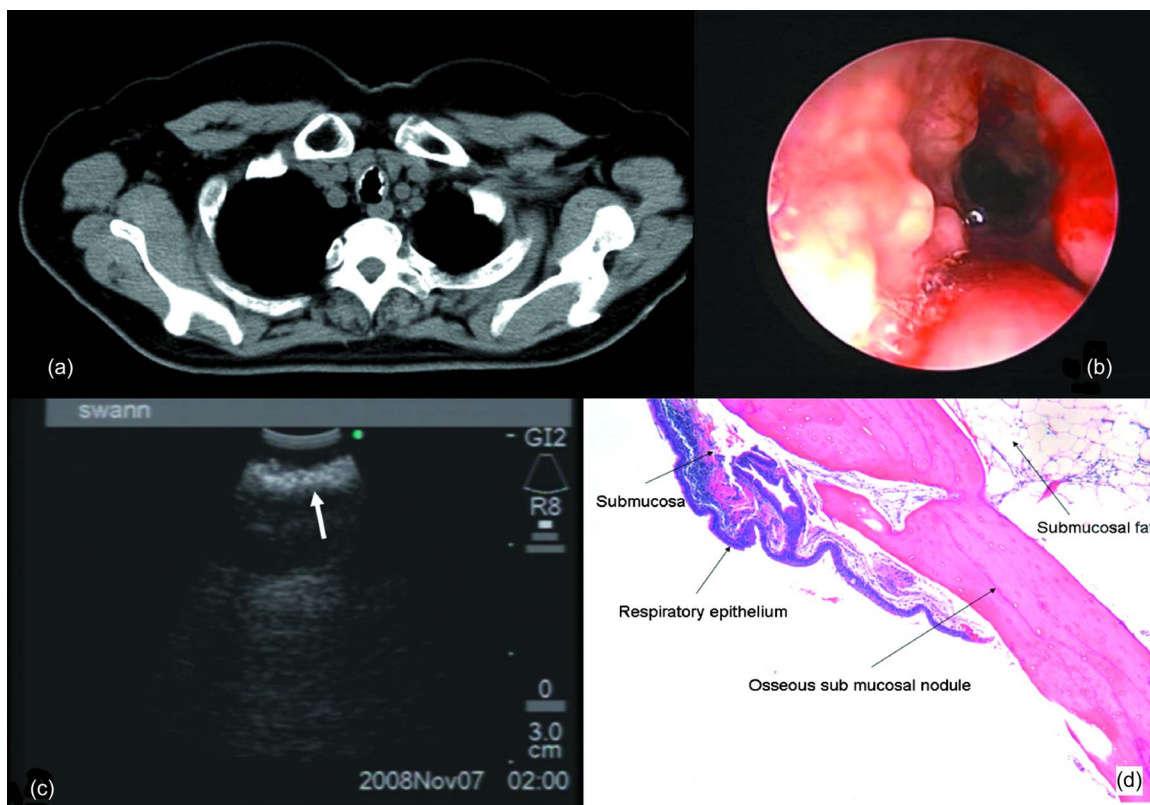
Fig. 1 (a) Computed tomography shows hyperdense nodular opacities along the anterior and lateral walls of the upper trachea. (b) While light bronchoscopy confirms firm, raised nodules along cartilaginous structures suggestive of TPO. (c) Cross-sectional EBUS image using convex 7.5-MHZ probe shows hyperechoic density of 0.4 cm thickness (white arrow) corresponding to the osseous submucosal nodule. (d) Histopathology from bronchoscopic biopsy: osseous submucosal nodules consisting of lamellar bone consistent with TPO. The overlying respiratory epithelium has focal squamous metaplasia (H & E stain magnification 5×).

eral resolution of 20–25 μm, focal distance set to facilitate use in the contact mode, imaging depth of 2.2 mm (in air), lateral scanning range of 2 mm, 0.67 fps for 200 lateral pixel images, and a probe diameter of 2.7 mm. Comparative images were obtained of normal-appearing tracheal mucosa and underlying cartilage (Fig. 2). Following multimodality imaging, biopsies using flexible forceps were attempted but were unsuccessful because of the firmness and fixation to cartilage of the nodules. Three-millimeter rigid cup forceps (Karl Storz, Culver City, California) were then used to obtain deep biopsies of the airway abnormalities. Histology showed ossification of the submucosa consistent with TPO [Fig. 1(d)].

3 Results

White-light bronchoscopy revealed irregularly shaped, firm submucosal nodules along cartilaginous structures of the anterior and lateral walls of the trachea, sparing the muscular posterior membrane [Fig. 1(b)]. Endobronchial ultrasound of one of the nodules showed a hyperechoic density of 0.4 cm thickness [Fig. 1(c)]. Because of limited depth resolution, endobronchial ultrasound did not show detailed anatomy. OCT identified respiratory epithelium, upper submucosa, and osseous submucosal nodule layers (Fig. 2) corresponding to histopathology [Fig. 1(d)].

4 Discussion

4.1 Overview of TPO

TPO, also known in the literature as tracheobronchopathica osteochondroplastica and tracheopathica osteoplastica, is a
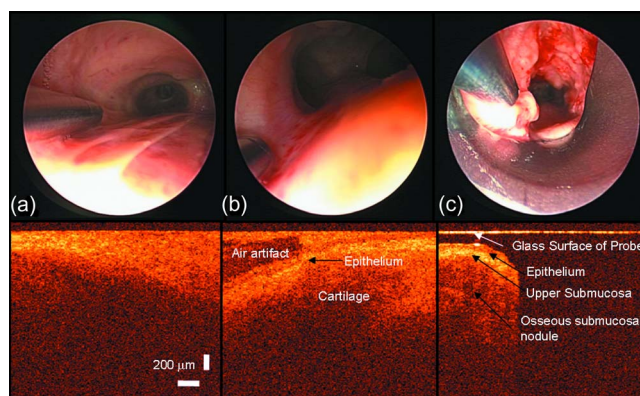
Fig. 2 Bronchoscopic images (upper row) showing inside-actuation frontal imaging probe overlying (a) normal tracheal mucosa and (b) normal cartilage as compared to the (c) thick, irregular, hyperdense nodular surface in TPO. The corresponding two-dimensional OCT images (lower row) reveal the respiratory epithelium, upper submucosa, cartilage and osseous submucosal nodule. Image size is 2 mm (horizontal) by 2.2 mm (in air, vertical).

rare nonmalignant disorder of the large airways characterized by multiple dense nodules localized in the submucosa of the tracheobronchial wall.[1] TPO is a slowly progressive disease of adulthood with a mean time from presentation to diagnosis of approximately four years, but its true incidence is unknown. TPO is usually detected incidentally upon intubation or when tomographic, magnetic resonance or bronchoscopic imaging is performed for airway symptoms or for unrelated conditions.[2–4]

Although TPO may involve the larynx, the disease is usually limited to the large central airways and does not involve the lung parenchyma or other organs. Mucosal changes, impaired ciliary clearance of secretions, and enlarged submucosal nodules may lead to recurrent inflammation, infection, and central airway obstruction. Cough, hoarseness, hemoptysis, exertional dyspnea, wheezing, and recurrent lower airway infections are usual symptoms. Stridor and rhonchi are present in advanced obstructive cases, which can lead to respiratory failure.[1]

The differential diagnosis for TPO includes nonmalignant processes, such as relapsing polychondritis, ulcerative colitis, amyloidosis, sarcoidosis, papillomatosis, and saber sheath trachea, but airway neoplasms must also be excluded.[5,6] The disease is usually distinguishable from other disorders, however, because it does not involve the posterior membranous portion of the trachea. Bronchoscopy is often considered to be pathognomonic when it reveals focal or diffuse raised, firm nodules overlying the cartilaginous rings. Biopsies are often difficult because of the bony nature of the nodules.[7,8]

Histopathologic studies suggest that bone morphogenetic protein 2 acts synergistically with transforming growth factor $\beta 1$, in the promotion of nodule formation within the tracheal submucosa.[8] Nodules are actually calcifications, chondrifications, or ossifications of the upper layer of the mucous membrane. These abnormalities may have foci of bone marrow with active areas of hemopoiesis. Ossifications are lamellar-type bone covered by normal mucosa or squamous metaplasia that may connect by bone, cartilage, or connective tissue to the perichondrium of the tracheal rings.[8] Although there is no obvious relationship with malignancy, a large case series from Japan showed that 24 (19%) of 126 patients had associated cancers, especially bronchogenic adenocarcinoma.[9] For this reason, bronchoscopic biopsies are usually performed even when TPO is the likely diagnosis.

4.2 Multimodality Imaging Clinical Applications

The future of multimodality bronchoscopic imaging resides on the premise that by combining appropriate resolutions and depth of penetrations of diverse technologies, characterization and diagnosis of benign, premalignant, and neoplastic abnormalities might be enhanced. Conventional white-light bronchoscopy is a sensitive, but usually nonspecific means with which to identify, locate, and biopsy gross airway mucosal abnormalities in up to fifth-generation segmental bronchi. It provides forward and angled surface visualization with a large field of view and depth of focus but does not allow cross-sectional imaging of bronchial and peribronchial tissues. Endobronchial ultrasound, on the other hand, which allows cross-sectional imaging of soft tissues, has been used to accurately measure depth of bronchial tumor invasion beyond the cartilaginous layers and allows identification of structural layers of the airway wall.[10]

Ultrasound is, however, limited in spatial resolution to approximately $50-200 \mu m$ due to long acoustic wavelengths. The standard frequency for radial probe endobronchial ultrasound (EBUS) is 20 MHz, which allows for a resolution of <1 mm, but with a depth of penetration of approximately 4–5 cm, allows for visualization of mediastinal structures, bronchial wall layers, and peribronchial lymphadenopathy or great vessels.[10,11] The conventional convex EBUS bronchoscope probe such as that used in this study has a frequency of only 7.5 MHz, allows for deeper penetration but with corresponding loss of resolution. Cartilaginous layers may be difficult to visualize but airway wall thickness can be measured *in vivo*. In fact, EBUS has been used to distinguish central airway wall structural abnormalities in patients with benign airway disorders, such as malacia caused by tuberculosis, relapsing polychondritis, and extrinsic compression by vascular rings,[12–14] identify structural differences in the membranous and cartilaginous portions of the central airways in patients with expiratory central airway collapse,[15] and potentially determine depth of endobronchial tumor invasion[16] which might help guide indications for open or bronchoscopic resection.

OCT is analogous to ultrasound B mode imaging, except that instead of using acoustic waves, it uses near-infrared light to measure reflected or backscattered light to produce high-resolution tomographic pictures. Using contact or noncontact probes, high-resolution OCT, such as that used in this study, is capable of up to two orders of magnitude greater resolution $(2-10 \mu m)$ than ultrasound at depths of up to ~2 mm in optically scattering tissues.[17] The depth range of OCT is therefore sufficient to penetrate through the upper layers of exposed tissues on airway surfaces, where many airway neoplasms or other airway pathology may present, and is equivalent to the tissue sampling depth of conventional endobronchial forceps.[18]

Clinical OCT systems consist of an imaging console and a detachable, flexible fiberoptic probe. Endoscopic OCT probes include an optical fiber with a compact scanner and are categorized into two-/three-dimensional imaging, side/front imaging, or outside/inside actuation depending on whether the scanner is outside the human body or located within the distal tip of the probe. To our knowledge, the smallest currently available probes can have a diameter of ~$400 \mu m$ (three-dimensional imaging, side imaging, and outside actuation).

In this study, we used a commercially available, compact time-domain OCT system (Niris System, Imalux Corp., Cleveland, Ohio) with a magnetically actuating probe (two-dimensional, front imaging, and inside actuation). The depth resolution is governed by the superluminescent laser diode bandwidth produced, and the ~15-μm resolution is enough to differentiate tissue layers using the endogenous contrast properties of the tissues. The lateral resolution is 25 μm with an imaging depth of 2.2 mm (in air). The probe, although small enough to access the human trachea and main carina, is too large to fit through the 2-mm working channel of a conventional flexible bronchoscope. Further reduction in probe diameter, however, may result in reduced lateral resolution. Because of the front-imaging feature, the lateral scanning range is, in fact, limited to 2 mm in the contact mode (where

Table 1 Comparison between the Niris and advanced OCT systems.

Research Group	Huber et al. (Ref. 19)	Potsaid et al. (Ref. 20)	Oh et al. (Ref. 21)	Niris System
Depth scan rate (kHz)	370	100	115	0.7
Axial resolution (in air) (μm)	13	2.5–3.0	13	10–20
Technology	Fourier domain (FDML based)	Fourier domain (spectrometer based)	Fourier domain (swept source based)	Time domain
FDA cleared for imaging human microsturcture	No	No	No	Yes

the focus is optimal and distance can be controlled) and probe positioning is difficult for visualizing the tracheal wall, though very straightforward for the main carina and other large-airway branching areas. The magnetic actuation method is capable of one-dimensional scanning only so that a three-dimensional tomographic image cannot be constructed. Although the magnetic actuation method, quick-connection/release mechanism, and waterproof design of the probe are unique, the Niris System utilizes time-domain technology, which limits A-scan rate capabilities compared to its Fourier-domain counterpart.

The comparison to advanced OCT systems in the literature is given in Table 1. Unidirectional sweep rates of 370 kHz over a 100-nm range at a center wavelength of 1300 nm can be achieved using Fourier-domain mode lock laser,[19] and high-speed, Fourier-domain OCT have demonstrated speeds of up to 370 kHz A-scan rate. Spatially encoded Fourier-domain technology using a high-speed camera has been reported.[20] This technology utilized a superluminescent diode with an 873 nm of center wavelength and a 144-nm full-width-at-half-maximum bandwidth or a femtosecond titanium sapphire laser. A-scan rate was 100 kHz, and depth resolution was 2.5–3.0 μm in air. A wavelength swept laser with a 115 kHz repetition rate was also developed[21] based on a polygon mirror filter and showing a depth resolution of 13 μm. The advantage of these Fourier-domain techniques is the ability to perform three-dimensional imaging within a few seconds. Data acquisition and processing speeds, however, are insufficient to use the full capacity of Fourier-domain techniques.

In conclusion, to our knowledge, this is the first time a commercially available time-domain OCT system is used as part of a multimodality bronchoscopy platform to study diagnostic imaging of a benign disease, such as TPO. Future OCT systems might be further optimized for such airway applications by developing smaller probes capable of insertion into standard 2.0- and 2.8-mm working channels of flexible bronchoscopes, longer sweep distances, broader wavelength laser sources with higher resolution capabilities, compact three-dimensional scanning, and integrated rapid Fourier-domain technologies.

References

1. K. Hussain and S. Gilbert, "Tracheopathia osteochondroplastica," *Clin. Med. Res.* **1**(3), 239–242 (2003).
2. F. J. Fernandez-Fernandez, M. J. Mejuto, G. Pia, J. Moreno, J. C. Alvarez, and M. D. Diaz-Miguez, "Massive hemoptysis associated with tracheopathia osteochondroplastica," *Ann. Med. Interne (Paris)* **13**(2), 73–74 (1996).
3. A. R. Birzgalis, W. T. Farrington, L. O'Keefe, and J. Shaw, "Localized tracheopathia osteoplastica of the subglottis," *J. Laryngol. Otol.* **107**(4), 352–353 (1993).
4. A. Neumann, D. Kasper, and H. J. Schultz-Coulon, "Clinical aspects of tracheopathia osteoplastica," *HNO* **49**(1), 41–47 (2001).
5. E. M. Marom, P. C. Goodman, and H. P. McAdams, "Diffuse abnormalities of the trachea and main bronchi," *AJR, Am. J. Roentgenol.* **176**(3), 713–717 (2001).
6. Y. Ohkubo, A. Narimatsu, M. Higuchi, K. Suzuki, A. Kohno, T. Shigeta, Y. Takizawa, and S. Nitta, "CT findings of the benign tracheobronchial lesions with calcification," *Rinsho Hoshasen* **35**(7), 839–846 (1990).
7. A. Mathlouthi, C. Ben Rehouma, S. Ben M'Rad, J. F. Dumon, N. Labbene, B. Driss, M. Sellami, and F. Djenayah, "Tracheobronchopathia osteochondroplastica. Personal observation and review of the literature," *Rev. Pneumol Clin.* **49**(3), 156–162 (1993).
8. R. Lazor and J. F. Cordier, "Tracheobronchopathia osteochondroplastica," *Orphanet Encyclopedia*, ⟨http://www.orpha.net/data/patho/GB/uk-TO.pdf⟩ (June 2004).
9. S. T. Yokoyama, "Bronchial science," *Jpn. Res. Inst. Bronch. Mag.* **18**, 558–562 (1996).
10. N. Kurimoto, "Diagnosis of depth penetration in the tracheobronchial tree," in *Endobronchial Ultrasonography*, N. Kurimoto, Ed., pp. 33–38, Kinpodo, Kyoto (2001).
11. N. Kurimoto, M. Murayama, S. Yoshioka, T. Nishisaka, K. Inai, and K. Dohi, "Assessment of usefulness of endobronchial ultrasonography in determination of depth of tracheobronchial tumor invasion," *Chest* **115**(6), 1500–1506 (1999).
12. Y. Iwamoto, T. Miyazawa, N. Kurimoto, Y. Miyazu, A. Ishida, K. Matsuo, and Y. Watanabe, "Interventional bronchoscopy in the management of airway stenosis due to tracheobronchial tuberculosis," *Chest* **126**(4), 1344–1352 (2004).
13. P. Lee, S. Low, H. Liew, D. Tan, and P. Eng, "Endobronchial ultrasound for detection of tracheomalacia from chronic compression by vascular ring," *Respirology* **12**(2), 299–301 (2007).
14. Y. Miyazu, T. Miyazawa, N. Kurimoto, Y. Iwamoto, A. Ishida, K.

Kanoh, and N. Kohno, "Endobronchial ultrasonography in the diagnosis and treatment of relapsing polychondritis with tracheobronchial malacia," *Chest* **124**(6), 2393–2395 (2003).

15. S. Murgu, N. Kurimoto, and H. Colt, "Endobronchial ultrasound morphology of expiratory central airway collapse," *Respirology* **13**(2), 315–319 (2008).

16. F. Herth, A. Ernst, M. Schulz, and H. Becker, "Endobronchial ultrasound reliably differentiates between airway infiltration and compression by tumor," *Chest* **123**(2), 458–62 (2003).

17. W. Drexler, U. Morgner, F. X. Kärtner, C. Pitris, S. A. Boppart, X. D. Li, E. P. Ippen, and J. G. Fujimoto, "*In vivo* ultrahigh-resolution optical coherence tomography," *Opt. Lett.* **24**(17), 1221–1223 (1999).

18. J. G. Fujimoto, M. E. Brezinski, G. J. Tearney, S. A. Boppart, B. Bouma, M. R. Hee, J. F. Southern, and E. A. Swanson, "Optical biopsy and imaging using optical coherence tomography," *Nat. Med.* **1**(9), 970–972 (1995).

19. R. Huber, D. C. Adler, and J. G. Fujimoto, "Buffered Fourier domain mode locking: unidirectional swept laser sources for optical coherence tomography imaging at 370,000 lines/s," *Opt. Lett.* **31**(20), 2975–2977 (2006).

20. B. Potsaid, I. Gorczynska, V. J. Srinivasan, Y. Chen, J. Jiang, A. Cable, and J. G. Fujimoto, "Ultrahigh speed spectral/Fourier domain OCT ophthalmic imaging at 70,000 to 312,500 axial scans per second," *Opt. Express* **16**(19), 15149–15169 (2008).

21. W. Y. Oh, S. H. Yun, G. J. Tearney, and B. E. Bouma, "115 kHz tuning repetition rate ultrahigh-speed wavelength-swept semiconductor laser," *Opt. Lett.* **30**(23), 3159–3161 (2005).